J. Am. Ceram. Soc., 99 [10] 3435–3442 (2016)
DOI: 10.1111/jace.14351

journal

The Effects of Low Oxygen Activity Conditions on the Phase Equilibria and Cation Occupancy of Strontium Barium Niobate

Jonathan A. Bock,[‡,†] Jason H. Chan,[‡] Yoed Tsur,[§] Susan Trolier-McKinstry,[‡] and Clive A. Randall[‡]

[‡]Materials Science and Engineering Department and Materials Research Institute, The Pennsylvania State University, University Park, Pennsylvania 16802

[§]Chemical Engineering Department, Technion – Israel Institute of Technology, Haifa 3200003, Israel

Strontium barium niobate (SBN) is a tungsten bronze family ferroelectric which shows promising thermoelectric properties under reducing conditions. It is found here that the enhanced electrical conductivity of oxygen-deficient SBN correlates with the formation of a NbO_2 secondary phase. The effects of the reducing environment and the NbO_2 phase formation are studied via a detailed defect chemistry analysis. Increasing amounts of the NbO_2 phase are accompanied by an interesting mechanism where the A-site occupancy of the SBN matrix increases. The resulting donor defects source the large carrier concentrations which cause the enhanced electrical conductivity necessary for thermoelectric performance. In investigation of the phase equilibria, it is found that a solid solution between $(Sr_{0.6}, Ba_{0.4})Nb_2O_6$ and $(Sr_{0.6},Ba_{0.4})_{1.2}Nb_2O_6$ exists and that the A-site filling is found to occur at more modest reduction conditions in Sr- and Ba-rich compositions. Finally, thermogravimetric analysis of the reoxidation process is performed, and the results suggest that the A-site filling is compensated ionically. Not only do the presented results explain the enhanced electrical conductivity of oxygen-deficient strontium barium niobate but also modification of the site occupancies by reduction and reoxidation may widen the design space for property modification in tungsten bronze-structured materials in general.

Keywords: *tungsten bronze; phase equilibria; thermoelectric; ferroelectric; point defects*

I. Introduction

Strontium barium niobate (SBN) is a ferroelectric material used in single crystal form for electro-optic and photorefractive nonlinear optic applications;[1,2] it has recently been identified as a potential thermoelectric in its oxygen-deficient state.[3–5] SBN has a tetragonal tungsten bronze structure with space group *P4bm* at room temperature[6] and the unit cell shown in Fig. 1. The formula unit can be represented as $(A1)_2(A2)_4C_4B_{10}O_{30}$ where both the A1 and A2 sites host strontium ions, barium ions sit exclusively on the A2 site, the C-site is empty, and Nb fills the B-sites inside the oxygen octahedra. Only five-sixth of the A1 and A2 sites are filled, resulting in an A-site vacancy solid solution which is thought to contribute to the relaxor ferroelectric properties of SBN.[6–9] Other tetragonal tungsten bronze materials show different cation site occupancies including, for example, in the 'stuffed' bronzes like $K_6Li_4Nb_{10}O_{30}$ where all of the A1, A2, and C-sites are completely filled,[10] and the "filled" bronzes like $Ba_4Na_2Nb_{10}O_{30}$ where the A1 and A2 sites are filled but the C-sites remain empty.[11] These differences in cation occupancy can be important to functional properties. For example, cation site occupancy influences the ferroelectric properties of tungsten bronzes, although research is ongoing as to the mechanism.[9,12] A recent survey of the field shows that the ordering of tilts may be a key parameter,[12] and changes in cation occupancy may affect these tilts.

Additionally, oxygen-deficient strontium barium niobate has been gaining interest as a potential thermoelectric material due to its low thermal conductivity and large thermoelectric power factor.[3–5,13–19] Research has focused on both benchmarking the thermoelectric performance[4,5,14,15] and understanding how the ferroelectric nature of SBN affects thermal conductivity[17,18] and electron transport.[3,19–21] Multiple researchers have noted the formation of an NbO_2 secondary phase in reduced SBN[3,13] and although the defect chemistry associated with oxygen loss in the SBN matrix is often considered,[5,13] other changes to the SBN matrix upon the formation of NbO_2 are not. As the electrical conductivity of NbO_2 is small compared to oxygen-deficient SBN[22], it is unlikely that this phase itself significantly enhances the thermoelectric performance. Despite this, samples with large electrical conductivities almost always show the formation of a NbO_2 phase.[13,19]

Understanding correlations between enhanced thermoelectric properties, the presence of NbO_2, and changes to the SBN matrix may give insights toward optimization of the thermoelectric performance of SBN. Here, the formation of the NbO_2 phase is studied as a function of annealing conditions with emphasis on changes to the A-site occupancy of the SBN matrix. The results show an increase in the A-site occupancy in SBN which explains the previously identified enhanced thermoelectric performance. The phase equilibria are then expanded into Sr/Ba-rich compositions. Finally, the ramifications of these findings on the oxidation resistance of SBN are discussed, and thermogravimetric analysis is used to study the reoxidation.

II. Experimental Procedure

Phase-pure $(Sr_{0.6}Ba_{0.4})Nb_2O_6$ powders were fabricated via solid-state reaction of $SrCO_3$, $BaCO_3$, and Nb_2O_5 powder precursors weighed out to the correct stoichiometric ratios and then heated to 1200°C for 6 h. The high temperatures and long dwell times for calcination are required to eliminate Nb-rich and Ba-poor regions which lead to abnormal grain growth via the creation of a liquid phase at 1240°C.[23] After ball-milling and drying of the reacted powder, pellets were uniaxially pressed at 15 MPa, cold isostatically pressed at 200 MPa, homogenized at 1200°C for 2 h, and sintered at 1325°C for 6 h to obtain >95% relative density.[19] Dense pellets were annealed at temperatures ranging from 950°C to

B. Raveau—contributing editor

Manuscript No. 38176. Received February 16, 2016; approved May 20, 2016.
[†]Author to whom correspondence should be addressed. e-mail: Jonathan.A.Bock@gmail.com

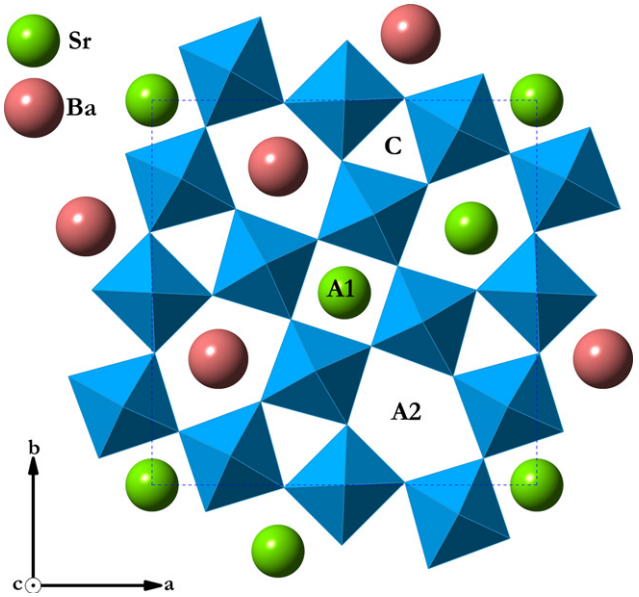

Fig. 1. Tetragonal tungsten bronze crystal structure of strontium barium niobate. Corner-shared NbO_6 octahedra connect in-plane to form multiple cation sites labeled as A1, A2, and C-sites. One-sixth of the A1 and A2 sites are empty in air-fired $(Sr_x,Ba_{1-x})Nb_2O_6$.

1300°C under oxygen partial pressures ranging from 10^{-9} to 10^{-19} atm. The phase compositions of samples were detected with powder X-ray diffraction (XRD) (PANalytical Empyrean Almeo, Netherlands).

An in-depth investigation was undertaken on a series of samples annealed at 1300°C and partial pressures of oxygen ranging from 10^{-9} to 10^{-16} atm. In these samples, changes in the chemistry of the SBN matrix were identified using quantitative energy-dispersive X-ray spectrometry (EDS) (FEI Quanta 200 Environmental SEM with an Oxford Instruments X-act 10 mm^2 silicon drift detector) to measure the (Sr+Ba):Nb ratio and Rietveld refinements were conducted to quantify the weight percentage of second phases in these samples. The refinements were conducted using PDF#04-0072133, #01-073-0487, and #04-002-9010 using JadeXRD analysis software. Samples for this investigation had compositions of $(Sr_{0.6}Ba_{0.4})Nb_2O_6$, $(Sr_{0.6}Ba_{0.4})_{1.1}Nb_2O_6$, and $(Sr_{0.6}Ba_{0.4})_{1.2}Nb_2O_6$ (SBN1.0, SBN1.1, and SBN1.2, respectively) and were fabricated using the same starting powders, calcining, and sintering conditions previously mentioned. Samples for EDS were polished down to 0.1 μm diamond slurry and samples were measured under a background pressure of 30 Pa to avoid charging of the sample surface. Electron beam intensity quantification was performed using copper foil and standardization of the EDS signal was performed using a phase-pure oxygen-deficient SBN1.0 pellet, which was annealed under 10^{-10} atm at 1300°C. Backscattered electron images were used to ensure that the EDS signal was only from the SBN matrix and to confirm the phase purity of XRD results.

Thermogravimetric analysis was performed on SBN1.0 samples annealed at 1300°C under 10^{-10} to 10^{-16} atm p_{O_2} using a TA 2050 (TA Instruments, New Castle, DE). Samples were heated in flowing air up to 800°C at 10°C/min using ~100 mg of powder. Sample pans were cleaned before each run by heating with an MAPP gas blowtorch.

Electrical conductivity tests were performed via a 4-pt probe measurement on rectangular samples of roughly 1.5 × 1.5 × 10 mm using a Integra 2700 multimeter (Keithley, Beaverton, OR). Sample leads were fabricated by sputtering platinum films through a shadow mask followed by attachment of silver wires by high-temperature silver epoxy. During measurement, samples were held under low oxygen partial pressure conditions to prevent reoxidation. Hall measurements on one SBN1.2 sample annealed at 10^{-16} atm were performed at 300 K using a PPMS system (Quantum Design, San Diego, CA). A Hall-bar geometry with Ga–In electrodes and silver wire leads were used. The Hall resistance was measured as a function of magnetic field from 80000 to −80000 Oe while a current of 5 mA AC source and a vacuum of 5 mTorr were maintained. The misalignment voltage was subtracted via use of magnetic field reversal.

III. Results and Discussion

(1) Conditions for NbO_2 Formation

Previous studies have identified the presence of the NbO_2 phase in oxygen-deficient SBN, but no studies have been conducted to precisely determine the annealing conditions necessary for NbO_2 formation. Therefore, the phase diagram of $(Sr_{0.6}Ba_{0.4})Nb_2O_{6-\delta}$ as a function of annealing temperature and oxygen partial pressure was investigated and is presented in Fig. 2. The NbO_2 phase forms when SBN is annealed at high temperatures under low oxygen partial pressures. As the annealing temperature is increased, the critical oxygen partial pressure for NbO_2 formation increases. This suggests that NbO_2 forms once SBN reaches a critical oxygen vacancy concentration. If so, then the one- and two-phase regions should be separable by a line of constant oxygen vacancy concentration in the SBN phase. The p_{O_2}-temperature conditions that control the thermodynamically stable concentration of oxygen vacancies can be calculated using the law of mass action assuming the defect reaction:

$$O_o^x \leftrightarrow V_o^{\cdot\cdot} + 2e^- + \frac{1}{2}O_{2(g)} \tag{1}$$

with an equilibrium constant of

$$K_{eq} = \frac{[V_o^{\cdot\cdot}]n^2 pO_2^{1/2}}{[O_o^x]} \tag{2}$$

where $[V_o^{\cdot\cdot}]$ is the oxygen vacancy concentration per oxygen lattice site, n is the electron concentration, $[O_o^x]$ is the concentration of oxygen per oxygen lattice site, and p_{O_2} is the partial pressure of oxygen used as a measure of the oxygen activity. When the following Brouwer approximation is employed:

$$n \cong 2[V_o^{\cdot\cdot}] \tag{3}$$

the p_{O_2}-temperature conditions are:

$$\ln(p_{O_2}) = \frac{2\Delta H}{RT} + \frac{2S_{conf}}{R} + 2\ln\left(\frac{[O_o^x]}{4[V_o^{\cdot\cdot}]^3}\right) \tag{4}$$

where: ΔH is the enthalpy of formation for an oxygen vacancy and S_{conf} is the configurational entropy. The vibrational entropy is assumed to be negligible as a first-order approximation. A line that separates the one- and two-phase regions is obtained with a ΔH of 4.25 eV and $[V_o^{\cdot\cdot}]$ of 0.002. These values are compatible with previous studies in SBN[24] and the TGA data in Fig. 7, discussed later. This condition is plotted as a dotted line in Fig. 2. The good agreement between Eq. 4 and the onset of NbO_2 formation suggest that the formation of NbO_2 is likely a result of the SBN reaching the solid solubility limit for oxygen vacancies. The result is that, under low partial pressures of oxygen, SBN leaves the solid solubility regime and enters a two-phase region resulting in the formation of NbO_2.

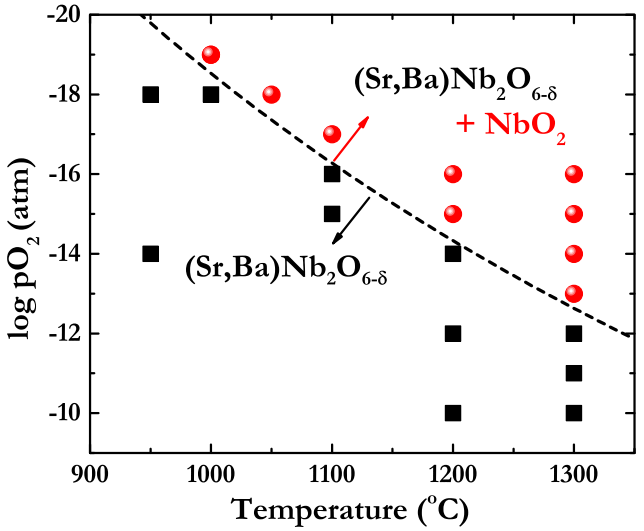

Fig. 2. Phase diagram of SBN at various annealing temperatures and partial pressures of oxygen. Black squares are phase-pure SBN within XRD detection limits, red circles correspond to a detectable amount of NbO_2. The dotted line shows a constant oxygen vacancy concentration assuming an oxygen vacancy formation enthalpy of 4.25 eV.

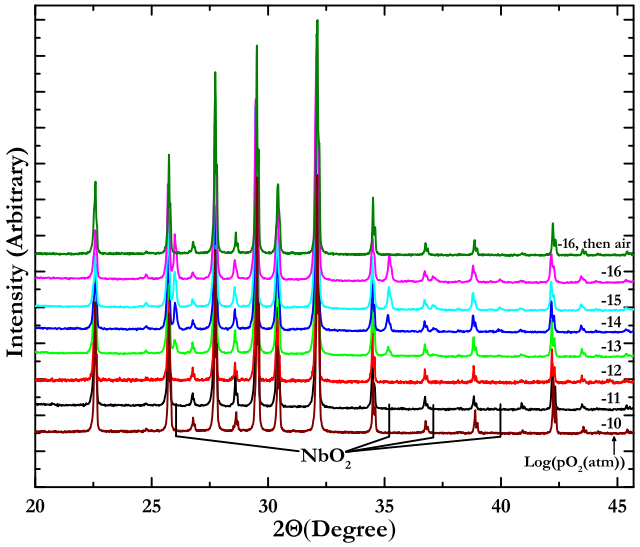

Fig. 3. Offset XRD patterns of $(Sr_{0.6},Ba_{0.4})Nb_2O_{6-\delta}$ annealed at 1300°C under multiple partial pressures of oxygen. The sample annealed at 10^{-16} atm p_{O_2} was reannealed in air at 1300°C, and shows only phase-pure SBN.

(2) Changes in Composition of SBN Matrix

Although a likely mechanism which determines the onset of NbO_2 formation has been identified, the mechanism by which enhanced thermoelectric properties occur must be established. Toward this goal, the changes to the chemistry of samples were studied. To understand the effect of NbO_2, it is important to note that the NbO_2 is the only secondary phase. That is, samples above the critical oxygen vacancy concentration threshold are mixtures of SBN and NbO_2 with no strontium-rich or barium-rich tertiary phases, as confirmed by XRD (e.g., Fig. 3) and scanning electron microscopy (SEM). The conservation of mass dictates that the total amounts of Sr, Ba, and Nb in the system must be kept constant before and after NbO_2 formation. There are two possible ways for this to occur without a Sr/Ba-rich tertiary phase. First, the excess Sr and Ba may either remain as defects in the SBN (and/or NbO_2) matrix or, secondly, the excess Sr and Ba may evaporate into the atmosphere as volatile species. The second possibility was eliminated by the following experiment: SBN+NbO_2 composites made by annealing at 1300°C under a p_{O_2} of 10^{-16} atm were reannealed in air at 1300°C for 6 h. The XRD pattern after the air anneal shows only a phase-pure SBN (Fig. 3) confirming the reversibility of the reaction. Similar results were verified for multiple SBN+NbO_2 composites. If extensive cation volatility occurred, then the Sr and Ba would not be present to reform phase-pure SBN. Extensive cation volatility is therefore ruled out, and the accommodation of the excess Sr and Ba is likely dominated by internal changes of the composition. A finite solubility of Nb (perhaps as Nb^{2+}) on the A-site is also possible. Clearly, however, this mechanism does not dominate the response, given the observation of NbO_2 second phase particles.

To investigate the changes in composition of the SBN matrix, quantitative EDS spectra were measured on the SBN matrix of SBN+NbO_2 composites formed at 1300°C under multiple p_{O_2} conditions. Due to charging under the electron beam, an unreduced insulating sample could not be used as a compositional standard. Quantification was instead achieved by presuming a phase-pure SBN sample annealed at 1300°C under 10^{-10} atm p_{O_2} to have a (Sr+Ba):Nb ratio of 0.5. The (Sr+Ba):Nb ratio of 0.5 was found to be maintained in phase-pure samples annealed at p_{O_2} values of 10^{-11} and 10^{-12} atm. As the partial pressure of oxygen during annealing is lowered, the (Sr+Ba):Nb ratio increases toward a value of 0.593 ± 0.015 [Fig. 4(a)]. The onset of NbO_2 formation occurs at 10^{-13} atm. This is the same condition under which the (Sr + Ba):Nb ratio first increases above 0.5. Both the (Sr+Ba):Nb ratio and the wt % of NbO_2 increase linearly as the partial pressure of oxygen decreases logarithmically below 10^{-12} atm p_{O_2} [Figs. 3 and 4(b)]. It therefore seems that the (Sr+Ba):Nb ratio and the NbO_2 phase formation are linked.

A link between NbO_2 concentration and the (Sr+Ba):Nb ratio could, in principle, be explained either by an increase in Nb vacancies or via an increase in the Sr and Ba concentration of the SBN matrix. The possibility of Nb vacancies can be ruled out based on the observation that the electrical conductivity rises as the (Sr+Ba):Nb ratio increases. As SBN is an *n*-type conductor,[19] acceptor defects such as Nb vacancies (which would promote *p*-type conductivity) are therefore unlikely. Thus, the exsolution of SBN into an SBN+NbO_2 composite must be accommodated by an increase in the Sr and Ba content in the SBN matrix. An increased A-site occupancy is a likely mechanism for this to occur.

In air-fired $(Sr_x,Ba_{1-x})Nb_2O_6$, only five of the six A1 and A2 sites (where Sr and Ba occupy) are filled, making SBN a vacancy solid solution with an A-site occupancy of 0.83. It is likely that the increase of the (Sr+Ba):Nb ratio is a result of the filling of these vacancies toward a limiting A-site occupancy of 1 and an end-member composition of $(Sr_xBa_{1-x})_{1.2}Nb_2O_6$. The formation of NbO_2 would therefore be a consequence of this process. As phase equilibria investigations of Sr–Ba–Nb–O systems show a finite solubility of excess Nb in SBN,[25,26] one possibility is that some of the excess Nb may remain in solution in the SBN matrix. The NbO_2 would therefore only form once the solubility limit for excess Nb in SBN is reached. The defect chemistry associated with the Nb excess is uncertain, but possibilities include Nb sitting on the A-site, similar to materials such as $Nb_{16}W_{18}O_{94}$[27,28] or possibly NbO-layer intergrowths as are found in multiple reduced niobates.[29–31] In the absence of any Nb excess in solution, the reaction for NbO_2 formation from an increasing A-site occupancy would be:

$$(1+y)(Sr_xBa_{1-x})Nb_2O_6 \rightarrow (Sr_xBa_{1-x})_{1+y}Nb_2O_6 + 2yNbO_2 + yO_{2(g)} \quad (5)$$

If Eq. 5 correctly describes the system, the wt% of NbO_2 in the final composite could be calculated once y is known;

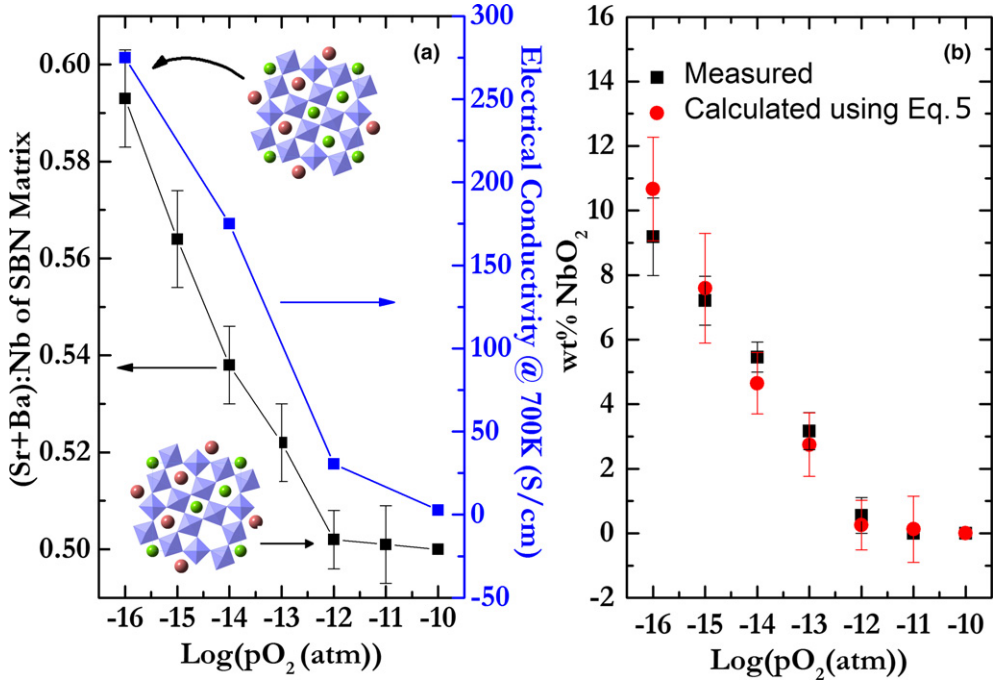

Fig. 4. (a) The (Sr+Ba):Nb ratio in the SBN matrix of SBN+NbO_2 composites increases alongside the electrical conductivity. (b) Eq. 5 correctly calculates the amount of NbO_2 formed using the (Sr+Ba):Nb ratio of the SBN matrix.

the value of y can be obtained using the (Sr+Ba):Nb ratio of the SBN matrix measured via EDS via:

$$\frac{(\mathrm{Sr}+\mathrm{Ba})}{\mathrm{Nb}} = \frac{(1+y)}{2} \tag{6}$$

This calculated wt% of NbO_2 is compared to the values measured via Rietveld refinements in Fig. 4(b) and shows good agreement. This suggests that Eq. 5 is appropriate, meaning that the NbO_2 formation is a response of the increased A-site occupancy and that Nb solubility is negligible within the error of the current measurements. Additionally, a sample annealed under 5% H_2/Ar forming gas at 1400°C was found to have an $SrNb_8O_{14}$-structured tertiary phase and an SBN matrix with a (Sr+Ba):Nb ratio of 0.597 ± 0.005. This agrees with a prediction of the A-site filling hypothesis that the maximum (Sr+Ba):Nb ratio should be 0.6, corresponding to an A-site occupancy of 1 with no excess Nb. After an A-site occupancy of 1 is reached, any additional decrease in the oxygen activity is accommodated by an additional phase. More accurate determination of the site occupancies could be achieved via Rietveld refinements as has been done previously for air-fired SBN,[6–8] but unlike previous studies, the A-site vacancy concentration must be refined in the current work. This additional degree of freedom renders refinements of the system unconstrained if only XRD and compositional analysis are used. Analysis of site occupancies using simultaneous refinement of X-ray and neutron diffraction data constrained via precise compositional analysis of the SBN matrix is an interesting avenue for future work.

From the perspective of oxygen-deficient SBN as a thermoelectric, the above finding suggests that engineering the carrier concentration for maximum thermoelectric performance is not a function of the concentration of oxygen vacancies only. The increased A-site occupancy can be treated as the filling of neutral A-site vacancies with 2+ cations or, in Kröger–Vink notation, $A_{V_A}^{\times\times}$. These defects must be taken into account when engineering the carrier concentration. For a filled SBN sample, the expected carrier concentration, n, can be calculated using the number of defects per unit cell, $6y$, and the volume of the unit cell from the lattice parameters. For $y = 0.2$, the completely filled condition, and a unit cell volume of 615 Å^3, the carrier concentration is calculated to be 4×10^{21}/cc. Such high carrier concentrations are near the degenerate regime, consistent with proposed impurity band models for electron transport in oxygen-deficient SBN.[19] Although previous studies assumed oxygen vacancies to be the major donor defect,[3,5] the difference of electrical conductivity before and after A-site filling starts to occur [2.8 S/cm in 10^{-10} atm samples compared to 275 S/cm in 10^{-16} atm samples, Fig. 4(a)] suggests that the oxygen vacancies play a minor role. The low partial pressures of oxygen during annealing seem to play the major role not by modifying the concentration of oxygen vacancies, but instead by moving the equilibrium into a phase region where A-site filling is favorable. It therefore seems that the correlation between the NbO_2 phase and enhanced thermoelectric properties occurs because the presence of NbO_2 is a marker for the onset of A-site filling. In this model, the NbO_2 is an unnecessary phase. Formulating compositions with various A-site occupancies without excess Nb may result in phase-pure samples with similarly enhanced thermoelectric properties.

(3) Phase Equilibria of $(Sr_{0.6},Ba_{0.4})_{1+y}Nb_2O_{6-\delta}$

To clarify the process of making phase-pure A-site filled samples, the phase equilibria of $(Sr,Ba)_{1+y}Nb_2O_{6-\delta}$ under low oxygen partial pressures were investigated. Two additional powders were batched with compositions equivalent to $(Sr_{0.6},Ba_{0.4})_{1.1}Nb_2O_6$ and $(Sr_{0.6},Ba_{0.4})_{1.2}Nb_2O_6$, or SBN1.1 and SBN1.2, respectively. Air-fired pellets of SBN1.1 and SBN1.2 were found to be mixtures of SBN and $(Sr_x,Ba_{1-x})_2Nb_2O_7$. The $(Sr_{1-x},Ba_x)_2Nb_2O_7$ in these pellets all were measured to be $x \approx 0.17$ via EDS, well within the solid solubility limits for $(Sr_{1-x},Ba_x)_2Nb_2O_7$ of $0 < x < 0.35$.[32] For simplicity, the notation "A" will be used to refer to cations that are either Sr^{2+} or Ba^{2+}. These air-fired pellets were annealed at 1300°C for 30 h at p_{O_2} values ranging from 10^{-9} to 10^{-16} atm, and the phase compositions were measured via XRD and Rietveld refinements.

The results are presented in Fig. 5. Three regions are found, one with only phase-pure SBN, one which shows the NbO_2 secondary phase, and another which shows an $A_2Nb_2O_7$ secondary phase. The dotted line which separates the phase-pure and SBN+$A_2Nb_2O_7$ region extends down to SBN1.0 in air. Given the results shown in Fig. 2, the boundary between the phase-pure SBN and SBN+NbO_2 regions is thought to be the solid solution limit for oxygen vacancies. The dotted line from Fig. 2 would therefore be the extension of this boundary into the temperature axis. From Gibbs' phase rule for this four component system, the number of degrees of freedom in the single-phase solid solution regime is five. The volumetric phase field in the quaternary diagram allows for independent changes in temperature, p_{O_2}, and the other three individual component chemical potentials. Once the solid solution limit of any component is reached, the system loses one degree of freedom and the chemical potentials can no longer be changed independently. This results in the two-phase regions in Fig. 5. For the SBN+NbO_2 phase region, both the amount of NbO_2 which forms and the composition of the SBN matrix would then be determined by the tie line between this phase boundary and the NbO_2 phase field on the Sr–Ba–Nb–O quaternary molar phase diagram. Similarly, the lower dotted line is thought to be the solid solution limit for partial Schottky defects; the phase composition would be determined by the tie line between this limit and the $A_2Nb_2O_7$ phase field boundary.

When the SBN phase is in equilibrium with a secondary phase, the chemical potentials of the different components are equal in both phases. This can be used to predict how the boundaries between the one- and two-phase regions react to changes in the component chemical potentials. For SBN-NbO_2 composites, this equilibrium results in:

$$2NbO_2 + \frac{1}{2}O_2 + A_{V_A}^{\ddot{x}} \leftrightarrow 2Nb_{Nb}^{x} + A_A^{x} + 5O_o^{x} + V_o^{\ddot{}} \quad (7)$$

This means, in terms of chemical potentials, that at the SBN-NbO_2 equilibrium:

$$\frac{1}{2}\mu(O_2) + \mu(A_{V_A}^{\ddot{x}}) = \text{const.} + \mu(V_o^{\ddot{}}) \quad (8)$$

As the oxygen vacancy solid solution limit has been reached, a decrease in the p_{O_2} cannot be accompanied by an increase in the $\mu(V_o^{\ddot{}})$. Hence, the result is an increased chemical potential for $A_{V_A}^{\ddot{x}}$. The increased chemical potential of Sr and Ba in SBN1.1 and 1.2 increases the $\mu(A_{V_A}^{\ddot{x}})$ and therefore decreases the $\mu(O_2)$, explaining the positive slope of the upper phase boundary in Fig. 5.

For SBN-$A_2Nb_2O_7$ composites at equilibrium:

$$A_2Nb_2O_7 \leftrightarrow 2Nb_{Nb}^{x} + A_A^{x} + 6O_o^{x} + \frac{1}{2}O_2 + A_{V_A}^{\ddot{x}} \quad (9)$$

and

$$\text{const.} = \frac{1}{2}\mu(O_2) + \mu(A_{V_A}^{\ddot{x}}) \quad (10)$$

Therefore, decreasing the oxygen partial pressure results in an increase in $\mu(A_{V_A}^{\ddot{x}})$ as confirmed by the positive slope of the lower phase boundary in Fig. 5. In both scenarios, an increase in the total (Sr+Ba):Nb ratio lowers the necessary oxygen activity for A-site filling.

The phase compositions of the samples are shown in Fig. 6 alongside the (Sr+Ba):Nb ratio of the SBN matrix measured via EDS. The amount of $A_2Nb_2O_7$ phase present in SBN1.1 and 1.2 is decreased compared to that of air-fired

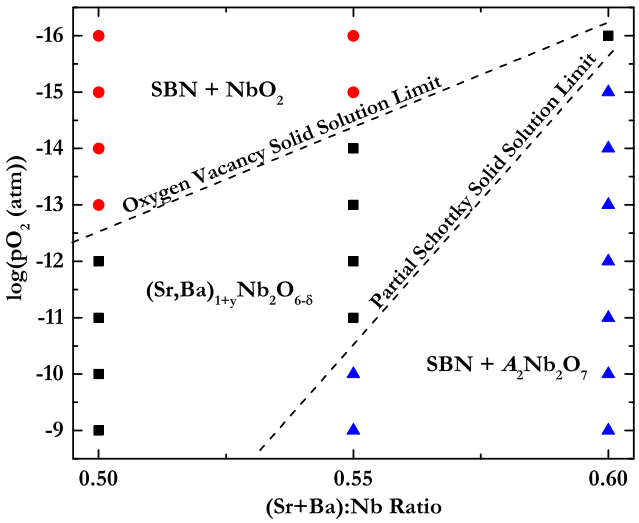

Fig. 5. Phase composition of different SBN samples batched with different (Sr + Ba):Nb ratios and annealed at 1300°C under various p_{O_2} conditions. Moving to the right on the plot corresponds to an increase in the Sr and Ba chemical potentials. Note that decreasing p_{O_2} is plotted along the positive y direction. Samples with NbO_2 as a secondary phase are marked with red circles, phase-pure samples are black squares, and samples with $A_2Nb_2O_7$ are blue triangles. The SBN phase region is limited by the solid solution limits of either oxygen vacancies or partial Schottky defects.

samples. This is corroborated by EDS data which shows the SBN matricies in SBN1.1 and 1.2 pellets possess a (Sr+Ba):Nb ratio above 0.5 for all samples. Therefore, SBN1.1 and 1.2 have increased A-site occupancy even at 10^{-9} atm p_{O_2}. This stands in stark contrast to SBN1.0, where changes to the A-site occupancy do not occur until 10^{-13} atm p_{O_2}. It does, however, agree with the predicted equilibrium between SBN and $A_2Nb_2O_7$ outlined in Eq. 10. Within the phase purity region of SBN1.1, the (Sr+Ba):Nb ratio of the SBN matrix remains constant near the expected value of 0.55. Changes in oxygen activity within these samples are accommodated by changes in the oxygen vacancy and quasi-free electron concentrations according to Eq. 2. This increased A-site filling in samples with increased strontium and barium contents point toward easier processing routes for thermoelectric SBN, as higher oxygen partial pressures may be used during annealing. The electron transport properties of these phase-pure filled SBN ceramics are similar to those of SBN+NbO_2 composites, and will be the topic of future publication.[33]

(4) Oxygen Absorption

From a device standpoint, the equilibrium conditions are important for processing, but more important is the stability of SBN under working conditions. Although filled SBN shows promise as a thermoelectric, the lack of oxidation resistance is a major hurdle which needs to be solved. The only quantitative numbers currently published show oxidation at temperatures as low as 700°C,[24] but changes in properties start to occur at much lower temperatures. It is widely mentioned in experimental procedures that high-temperature measurements of SBN are performed under inert atmospheres,[14,15,19] and polycrystalline SBN samples measured in 0.1 atm He above 480°C were reported to show degradation of the electrical properties.[19]

Given the current results on A-site filling, the sensitivity of the electrical properties of SBN to oxygen environments is peculiar. As discussed previously, a vast majority of the carrier concentration is thought to occur due to the A-site donors rather than the compensation of oxygen vacancies.

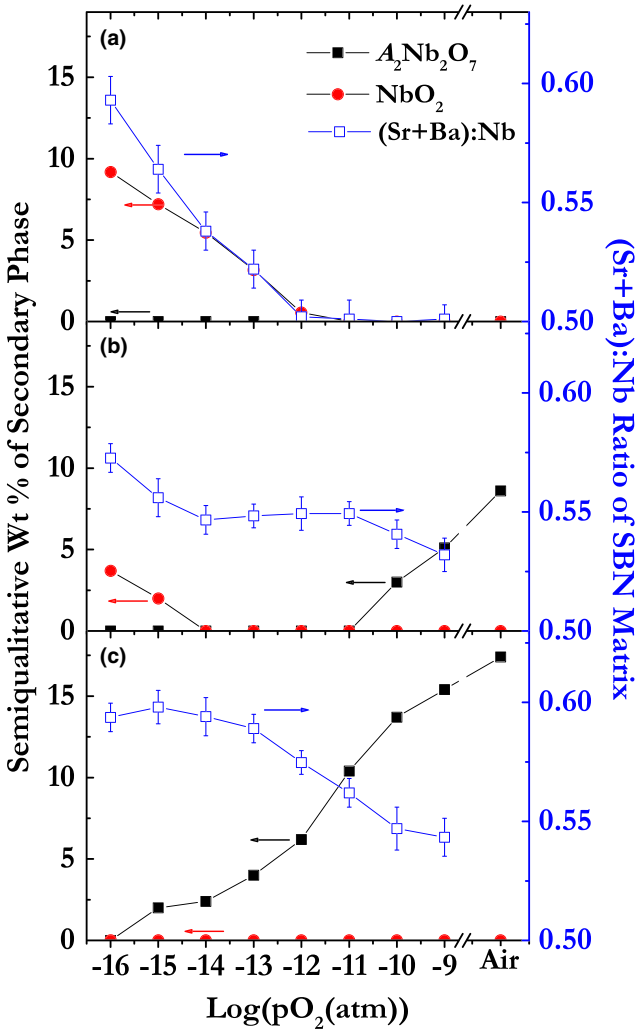

Fig. 6. Phase composition of SBN samples batched with a (Sr+Ba):Nb ratio of (a) 0.50 (b) 0.55, and (c) 0.60 annealed at 1300°C at varying p_{O_2} conditions. The amount of $A_2Nb_2O_7$ drops below that of air-fired samples at p_{O_2} values as low as 10^{-9} atm, showing that A-site filling is occurring at higher p_{O_2} values in samples with increased (Sr+Ba):Nb ratios.

While the oxygen vacancies may be filled via annealing in air, the A-site donors should remain, and therefore require a negative compensating defects such as electrons. However, oxygen-deficient SBN annealed under 10^{-16} atm was annealed in air at 700°C for 3 h and resulted in a white powder of SBN and γ-Nb_2O_5. The white color of the powder points toward a lack of electronic carriers, suggesting the A-site donors must be ionically compensated. The defect chemistry for the ionic compensation scenario is puzzling, as the possible compensating defects are either cation vacancies or some form of superoxidation. Both of these are unlikely. Under the equilibrium condition in air, the A-site donors would either react with NbO_2 to form SBN (for SBN1.0) or form an $A_2Nb_2O_7$ phase (for higher Sr and Ba concentrations). However, for the kinetically constrained condition of annealing at 700°C, it is unlikely that cations could migrate long distances. If the required 10^{21}/cc cation vacancies did form, then the aforementioned secondary phases would be detectable via SEM or XRD (either as a crystalline phase or an amorphous hump), and no evidence of such a secondary phase is found. Therefore, migration of the A-site donors out of the lattice is unlikely.

The sluggish cation motion means that compensation occurs via the anion lattice. However, the formation of oxygen interstitials is unlikely due to their large size. The largest empty site in A-site-filled SBN is the C-site. Outside of the fact that an oxygen interstitial on this site would be unfavorably surrounded by anions, the only ion which has been found to fit on the C-site is Li^+,[10] which has a 6-coordination Shannon-Prewitt radius of 0.74 Å, much smaller than the radius of 1.40 Å for an oxygen anion in 6-coordination. Due to this, it is unclear where the additional oxygen absorption is located or the mechanism by which it occurs. The peculiar nature of this A-site donor compensation makes the identification and study of any possible oxygen absorption via TGA is worthwhile.

The results from TGA are presented in Fig. 7. A measurable weight gain is present and clearly increases for samples which are annealed under lower oxygen activities. Care must be taken in analysis of the TGA data as it is a result of two contributions. One contribution is from the NbO_2 to Nb_2O_5 transition and the other from absorption of oxygen by the SBN matrix. However, these may be deconvoluted to a degree. This is because the amount of NbO_2 in the samples is known from the Rietveld refinements discussed previously. Unfortunately, a combination of errors from both the wt% of NbO_2 from Rietveld refinements and the baseline drift in the TGA signal prevents precise deconvolution of the two contributions, but rough estimates are possible. The calculated weight gain from the NbO_2 to Nb_2O_5 transition is $128\ \frac{mg}{gNbO_2}$, giving an expected weight gain of 0.6 ± 0.1% for SBN1.0 annealed under 10^{-16} atm p_{O_2}. This accounts for only roughly half of the measured weight gained. The remainder must be due to absorption of oxygen by the SBN matrix.

The oxygen absorption by the SBN matrix could be from either filling of oxygen vacancies and/or superoxidation. The samples with neither A-site filling nor NbO_2 ($10-^{11}$ and $10-^{12}$ atm pO_2), show no measureable weight gain discernable from the baseline drift of the TGA. The 10^{-12} atm sample is near the solid solubility limit for oxygen vacancies, and therefore its weight gain should estimate the maximum weight gain from oxygen vacancies possible in any sample. As this weight gain is <0.1% (i.e., lower than TGA can measure), it is thought that the contribution to the weight gain from the filling of oxygen vacancies is minimal. The additional absorption of oxygen in the SBN lattice must therefore be due to some form of superoxidation. The location of the excess oxygen is unknown and outside of the scope of this

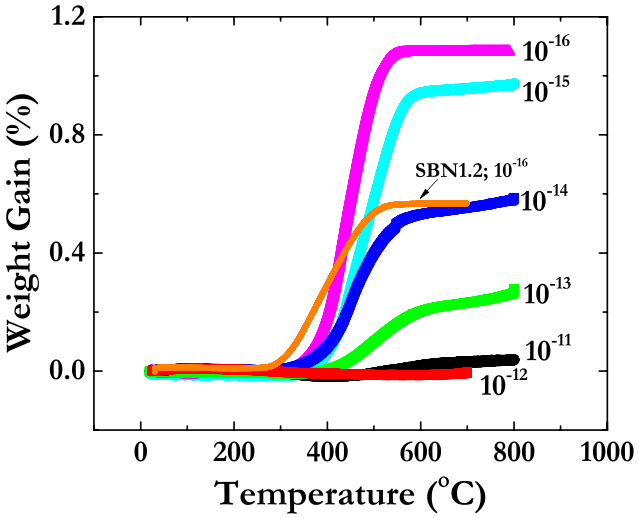

Fig. 7. Thermogravimetric analysis in air of various $(Sr_{0.6}Ba_{0.4})Nb_2O_6$ powders annealed at 1300°C for different partial pressures of oxygen (in atm). The weight gain is a combination of an NbO_2 to Nb_2O_5 transition and the changing oxygen content of the matrix. The weight gain increases with decreasing partial pressure of oxygen during annealing.

manuscript, but for simplicity, an absorbed oxygen with a 2^- charge will be denoted as an oxygen interstitial, $[O_i'']$.

The electroneutrality equation for SBN during low-temperature reoxidation is then:

$$2[A_{V_A^x}^{\cdot\cdot}] + 2[V_o^{\cdot\cdot}] = n + 2[O_i''] \quad (11)$$

Under the fully oxidized condition, $[V_o^{\cdot\cdot}]$ is negligible and samples are insulating and white, suggesting n is negligible as well. Therefore, for oxidized samples, we may write:

$$2[A_{V_A^x}^{\cdot\cdot}] \cong 2[O_i''] \quad (12)$$

Thus, under these conditions, the weight gain of the SBN matrix during reoxidation is entirely due to the superoxidation, $[O_i'']$. As the amount of superoxidation can be determined via the weight gain measured via TGA, the $[A_{V_A^x}^{\cdot\cdot}]$ can be determined via Eq. 12. For the TGA data in Fig. 7, the concentrations lay in the range of ~10^{21}/cc. This result can be used to measure the carrier concentration of oxygen-deficient samples. This is because, in oxygen-deficient samples, it can be assumed $[O_i''] = 0$ and $[A_{V_A^x}^{\cdot\cdot}] \gg [V_o^{\cdot\cdot}]$ resulting in Eq. 11 simplifying to:

$$2[A_{V_A^x}^{\cdot\cdot}] \cong n \quad (13)$$

As $[A_{V_A^x}^{\cdot\cdot}]$ was measured to be ~10^{21}/cc using Eqs. 12, the subsequent use of Eq. 13 suggests that the carrier concentration of reduced SBN is ~10^{21}/cc. This carrier concentration is close to the expected carrier concentration of 4×10^{21}/cc from complete A-site filling, calculated previously.

Precise determination of n is hindered by the previously mentioned errors from TGA and Rietveld refinements associated with the NbO_2 phase. A more accurate determination of n is possible if the same analysis is performed on a phase-pure SBN1.2 sample annealed at 1300°C under forming gas. The value of n in this sample was determined by two methods. First, by assuming the weight gain during TGA was due to superoxidation and then using Eq. 12 and Eq. 13 to calculate n. Secondly, carrier concentrations were determined on reduced samples by Hall measurements. The TGA data for the SBN1.2 sample is presented alongside the TGA data for SBN1.0 in Fig. 7. The value of n calculated from TGA was found to be $(2.6 \pm 0.3) \times 10^{21}$/cc. Hall measurements on this sample before reoxidation gave a value for n of $(2.3 \pm 0.3) \times 10^{21}$/cc. The equivalence of these numbers suggests that the analysis of Eq. 11 through Eq. 13 is correct. From these results, it seems that the lack of oxidation resistance is not due to the filling of oxygen vacancies, but instead to the absorption of additional oxygen. Additional research is necessary to identify the specific location of this oxygen in the lattice. Knowledge of the oxygen position could help in identifying a strategy for increasing the oxidation resistance of SBN thermoelectrics. As a final point, the lack of an NbO_2 phase in the SBN1.2 sample meant that the sample did not powderize due to the NbO_2 to Nb_2O_5 transition upon reoxidation. The dielectric properties of reoxidized ceramic samples were therefore measureable and were found to change significantly from air-fired SBN as is discussed elsewhere.[33] Effects of the increased A-site occupancy and superoxidation on the structure–property relations of tetragonal tungsten bronze dielectrics is an interesting avenue for future work.

IV. Summary

Formation of NbO_2 occurs in oxygen-deficient SBN at high temperatures and low partial pressures of oxygen once a critical oxygen vacancy concentration is reached. As the oxygen activity decreases at a constant temperature, the amount of NbO_2 increases and is accompanied by an increase in the (Sr+Ba):Nb ratio of the SBN matrix. It is shown that the defect mechanism for this change is the filling of the naturally occurring A-site vacancies in SBN, a mechanism which results in donor defects. Using the chemical potential equivalence of cations between the matrix and secondary phase, it is shown that increasing the (Sr+Ba):Nb in the starting batch results in an increased chemical potential for A-site stuffing and affects the critical oxygen activity for second-phase formation. This provides an interesting route toward control of the carrier concentration in thermoelectric SBN via the A-site filling. The lack of oxidation resistance of SBN under this model is due to compensation of $[A_{V_A^x}^{\cdot\cdot}]$ by some form of superoxidation. All in all, the current results show an interesting crystal-chemical modification of SBN due to processing in low partial pressures of oxygen. The tungsten bronze structure possesses a large number of degrees of freedom which allows for property design, and this new processing route widens the design space. This helps not only to increase the utility of oxygen-deficient SBN as a thermoelectric, but should also be a useful tool in building a set of structure–property relations of tungsten bronzed structured materials.

Acknowledgments

This research was supported by the United States-Israel Binational Science Foundation (BSF-Energy) grant number 2011510, and the National Science Foundation grant numbers IIP-1361571 and DMR-1206518. Y.T. wishes to thank the Nancy and Stephen Grand Technion Energy Program (GTEP). Thanks also goes to Soonil Lee and Takashi Teranishi for providing the groundwork for Fig. 1.

References

[1]M. D. Ewbank, R. R. Neurgaonkar, W. K. Cory, and J. Feinberg, "Photorefractive Properties of Strontium-Barium Niobate," *J. Appl. Phys.*, **62** [2] 374–80 (1987).

[2]S. Sakamoto and T. Yazaki, "Anomalous Electro-Optic Properties of Ferroelectric Strontium Barium Niobate and Their Device Applications," *Appl. Phys. Lett.*, **22** [9] 429–31 (1973).

[3]S. Lee, J. A. Bock, S. Trolier-McKinstry, and C. A. Randall, "Ferroelectric-Thermoelectricity and Mott Transition of Ferroelectric Oxides With High Electronic Conductivity," *J. Eur. Ceram. Soc.*, **32** [16] 3971–88 (2012).

[4]S. Lee, S. Dursun, C. Duran, and C. A. Randall, "Thermoelectric Power Factor Enhancement of Textured Ferroelectric $Sr_xBa_{1-x}Nb_2O_{6-\delta}$ Ceramics," *J. Mater. Res.*, **26** [01] 26–30 (2011).

[5]S. Lee, R. H. T. Wilke, S. Trolier-McKinstry, S. Zhang, and C. A. Randall, "$Sr_xBa_{1-x}Nb_2O_{6-\delta}$ Ferroelectric-Thermoelectrics: Crystal Anisotropy, Conduction Mechanism, and Power Factor," *Appl. Phys. Lett.*, **96** [3] 031910 (2010).

[6]P. B. Jamieson, S. C. Abrahams, and J. L. Bernstein, "Ferroelectric Tungsten Bronze-Type Crystal Structures. I. Barium Strontium Niobate $Ba_{0.27}Sr_{0.75}Nb_2O_{5.78}$," *J. Chem. Phys.*, **48** [11] 5048–57 (1968).

[7]M. P. Trubelja, E. Ryba, and D. K. Smith, "A Study of Positional Disorder in Strontium Barium Niobate," *J. Mater. Sci.*, **31**, 1435–43 (1996).

[8]J. G. Carrio, Y. P. Mascarenhas, W. Yelon, I. A. Santos, D. Garcia, and J. A. Eiras, "Structure Refinement of $(Sr,Ba)Nb_2O_6$ Ceramic Powder from Neutron and X-Rays Diffraction Data," *Mater. Res.*, **5** [1] 57–62 (2002).

[9]C. J. Huang, K. Li, X. Q. Liu, X. L. Zhu, and X. M. Chen, "Effects of A1/A2-Sites Occupancy Upon Ferroelectric Transition in $Sr_xBa_{1-x}Nb_2O_6$ Tungsten Bronze Ceramics," *J. Am. Ceram. Soc.*, **97** [2] 507–12 (2014).

[10]S. C. Abrahams, P. B. Jamieson, and J. L. Bernstein, "Ferroelectric Tungsten Bronze-Type Crystal Structures. III. Potassium Lithium Niobate $K_{6-x-y}Li_{4+x}Nb_{10+y}O_{30}$," *J. Chem. Phys.*, **54** [6] 2355–67 (1971).

[11]P. B. Jamieson, S. C. Abrahams, and J. L. Bernstein, "Ferroelectric Tungsten Bronze-Type Crystal Structures. II. Barium Sodium Niobate $Ba_{4+x}Na_{2-2x}Nb_{10}O_{30}$," *J. Chem. Phys.*, **50** [1969] 4352–63 (1969).

[12]X. Zhu, M. Fu, M. C. Stennett, P. M. Vilarinho, I. Levin, et al., "A Crystal-Chemical Framework for Relaxor Versus Normal Ferroelectric Behavior in Tetragonal Tungsten Bronzes," *Chem. Mater.*, **27** [9] 3250–61 (2015).

[13]C. S. Dandeneau, Y. Yang, B. W. Krueger, M. A. Olmstead, R. K. Bordia, and F. S. Ohuchi, "Site Occupancy and Cation Binding Sites in Reduced Polycrystalline $Sr_xBa_{1-x}Nb_2O_6$," *Appl. Phys. Lett.*, **104**, 101607 (2014).

[14]C. S. Dandeneau, T. W. Bodick, R. K. Bordia, and F. S. Ohuchi, "Thermoelectric Properties of Reduced Polycrystalline $Sr_{0.5}Ba_{0.5}Nb_2O_6$ Fabricated Via Solution Combustion Synthesis," *J. Am. Ceram. Soc.*, **96** [7] 2230–7 (2013).

[15]Y. Li, J. Liu, C. Wang, W. Su, Y. Zhu, et al., "Effects of Oxygen-Reduction on Thermoelectric Properties of $Sr_{0.61}Ba_{0.39}Nb_2O_6$ Ceramics," *Mater. Sci. Forum*, **787**, 210–14 (2014).

[16]Y. Chang, S. Lee, S. Poterala, C. A. Randall, and G. L. Messing, "A Critical Evaluation of Reactive Templated Grain Growth (RTGG) Mecanisms in Highly [001] Textured $Sr_{0.61}Ba_{0.39}Nb_2O_6$ Ferroelectric-Thermoelectrics," *J. Mater. Res.*, **26** [24] 3044–50 (2011).

[17]Y. Li, J. Liu, Y. Hou, Y. Zhang, Y. Zhou, et al., "Thermal Conductivity and Thermoelectric Performance of $Sr_xBa_{1-x}Nb_2O_6$ Ceramics at High Temperatures," *Scr. Mater*, **109**, 80–3 (2015).

[18]T. Kolodiazhnyi, H. Sakurai, O. Vasylkiv, H. Borodianska, and Y. Mozharivskyj, "Abnormal Thermal Conductivity in Tetragonal Tungsten Bronze $Ba_{6-x}Sr_xNb_{10}O_{30}$," *Appl. Phys. Lett.*, **104** [11] 111903 (2014).

[19]J. A. Bock, S. Trolier-McKinstry, G. D. Mahan, and C. A. Randall, "Polarization-Based Perturbations to Thermopower and Electronic Conductivity in Highly Conductive Tungsten Bronze Structured $(Sr,Ba)Nb_2O_{6-\delta}$," *Phys. Rev. B*, **90** [11] 115106 (2014).

[20]C. S. Dandeneau, Y. Yang, M. A. Olmstead, R. K. Bordia, and F. S. Ohuchi, "Polaronic Conduction and Anderson Localization in Reduced Strontium Barium Niobate," *Appl. Phys. Lett.*, **107** [23] 232901 (2015).

[21]T. Kolodiaznyi, H. Sakurai, M. Isobe, Y. Matsushita, S. Forbes, et al., "Superconductivity and Crystal Structure Origins of the Metal-Insulator Transition in $Ba_{6-x}Sr_xNb_{10}O_{30}$ Tetragonal Tungsten Bronzes," *Phys. Rev. B*, **92** [21] 214508 (2015).

[22]R. F. Janninck and D. H. Whitmore, "Electrical Conductivity and Thermoelectric Power of Niobium Dioxide," *J. Phys. Chem. Solids*, **27**, 1183–7 (1966).

[23]H.-Y. Lee and R. Freer*f*, "Abnormal Grain Growth and Liquid-Phase Sintering in $Sr_{0.6}Ba_{0.4}Nb_2O_6$ (SBN40) Ceramics," *J. Mater. Sci.*, **33** [7] 1703–8 (1998).

[24]C. S. Dandeneau, *"Defect Chemistry and Thermoelectric Behavior of n*-Type $(Sr_xBa_{1-x})Nb2O6$" M. S. Thesis. University of Washington, Seattle, WA, 2015.

[25]J. R. Carruthers and M. Grasso, "Phase Equilibria Relations in the Ternary System BaO-SrO-Nb_2O_5," *J. Electrochem. Soc.*, **117** [11] 1426–30 (1970).

[26]C. Nikasch and M. Gobbels, "Phase Relations and Lattice Parameters in the System SrO-BaO-Nb_2O_5 Focusing on SBN $(Sr_xBa_{1-x}Nb_2O_6)$," *J. Cryst. Growth*, **269** [2–4] 324–32 (2004).

[27]A. W. Sleight, "The Crystal Structure of $Nb_{16}W_{18}O_{94}$, a Member of a $(MeO)_xMeO_3$ Family of Compounds," *Acta Chem. Scand.*, **20**, 1102–12 (1966).

[28]C. P. Heinrich, M. Schrade, G. Cerretti, I. Lieberwirth, P. Leidich, et al., "Tetragonal Tungsten Bronzes Nb8-XW9 + XO47-δ: Optimization Strategies and Transport Properties of a new n-Type Thermoelectric Oxide," *Mater. Horiz.*, **47**, 519–27 (2015).

[29]G. Svensson, "X-Ray Diffraction and Electron Microscopy Studies of New Reduced Phases in the Ba-Nb-O System," *Solid State Ionics*, **32**, 126–33 (1989).

[30]G. Svensson, "$Ba_2Nb_5O_9$ - An Intergrowth of $BaNbO_3$ (Perovskite) and NbO," *Mat. Res. Bull.*, **23**, 437–46 (1988).

[31]G. Svensson, "HREM Sutdies of Introgrwoth Between NbO and Perovskite in the Ba,Sr and K-Nb-O Systems," *Micros. Microanal. Microstruct.*, **1**, 343–56 (1990).

[32]V. M. Zhukovsky and A. L. Podkorytov, "Investigation of s,p,d-Element Niobated and Their Solid Solution Formation Processes by Thermal Analysis," *J. Therm. Anal. Calorim.*, **60**, 523–34 (2000).

[33]J. Chan, "*Study of Filled Tungsten Bronze Strontium Barium Niobate for Thermoelectric Applications"; M. S. Thesis*. The Pennsylvania State University, Park, PA, 2016. □